Journal of Alloys and Compounds 509 (2011) 5755–5760

Contents lists available at ScienceDirect

Journal of Alloys and Compounds

journal homepage: www.elsevier.com/locate/jallcom

Nano-sized Y_2O_3:Eu^{3+} hollow spheres with enhanced photoluminescence properties

Ying Xiao, Dapeng Wu, Yi Jiang, Ning Liu, Junli Liu, Kai Jiang*

College of Chemistry and Environmental Science, Henan Normal University, Henan, Xinxiang 453007, PR China

ARTICLE INFO

Article history:
Received 31 August 2010
Received in revised form
17 December 2010
Accepted 17 December 2010
Available online 24 December 2010

Keywords:
Nanostructured materials
Chemical synthesis
Sintering
Optical properties

ABSTRACT

Nano-sized Y_2O_3:Eu^{3+} hollow spheres were fabricated via a facile strategy including preparation of the hollow precursor and a later calcination. Moreover, the growth process of these hollow spheres was monitored by time-dependent experiments and their luminescence properties were also intensively studied. The products exhibit strong red emitting at 613 nm under ultraviolet excitation and control experiments were carried out to optimize the synthetic conditions. It was found 850 °C calcination with 9 mol% doping level could give out the best photoluminescence performance. Moreover, a possible mechanism for the enhanced PL performance was also proposed based on the FT-IR investigation.

1. Introduction

As a main and unsurpassed red emitting material in fluorescent lamps and flat panel devices, europium-doped yttrium oxide (Y_2O_3:Eu^{3+}) has attracted extensive attention. It has many advantages such as short decay time, high quantum efficiency, good color coordination, excellent stability and avoidance of hazardous constituents [1–4]. Therefore, many strategies have been developed to synthesize Y_2O_3:Eu^{3+} materials including coprecipitation, combustion, spray pyrolysis, sol–gel and hydrothermal method [5–9]. Moreover the morphologies of this material were also tailored to manipulate its optical performance such as Y_2O_3:Eu^{3+} film prepared through direct oxidation, nanobelts synthesized by solvothermal process and hexagonal microprisms fabricated through microwave-assisted method [10–12]. However, these methods generally involved tedious process, rigid condition and hazardous starting material, which are unfavorable for scale up.

Due to the structural advantages, hollow materials have many potential applications in the fields such as photonic device, drug delivery, active-materials protection, and catalysis [13–19]. Therefore, considerable researches have been focused on the fabrication of these materials. Although template directing is the most straightforward method, this strategy suffers from many disadvantages including high cost and complicated procedures. Thus, one-pot and template-free methods are more attractive and feasible to produce hollow-structured materials [20–24]. Though many efforts have been exerted, it still remains a challenge to obtain hollow structures with uniform morphology and narrow size distribution. On the other hand, rare earth based materials with hollow interior reduce the usage of expensive rare elements, which could substantially cut down the cost. However, except a few examples, the synthesis of well-defined rare earth oxide hollow spheres was seldom reported previously [5,25,26].

In this work, hollow spherical precursor (300 nm in diameter) was firstly prepared via solvothermal method using ethanol and water (4/3 volume ratio) as solvents. During this synthesis, yttrium (europium) nitrate and urea were adopted as starting materials. Based on the time dependent experiments, urea was found to play a crucial role in inducing and directing the growth of hollow-structured precursor. Subsequently, the as-prepared precursor was annealed in air to generate Y_2O_3:Eu^{3+} hollow structures. In addition, the photoluminescence (PL) properties of the Y_2O_3:Eu^{3+} products prepared under different conditions were investigated. It was found the optimal calcination temperature and doping level are 850 °C and 9 mol% respectively. Compared with previous reports, the current method is simple, low cost and could be potentially adopted as a general strategy to fabricate other hollow structures.

2. Experimental

2.1. Synthesis of precursor hollow spheres

In a typical synthesis, 0.36 g of urea, 2.5 mL 0.2 M $Y(NO_3)_3{\cdot}6H_2O$ and $Eu(NO_3)_3{\cdot}6H_2O$ with Eu^{3+} doping level ranging from 1 mol% to 13 mol% were dissolved in mixture solution of absolute ethanol and deionized water (v/v = 4:3). Then

* Corresponding author. Tel.: +86 373 3326209; fax: +86 373 3326209.
E-mail address: jiangkai6898@126.com (K. Jiang).

0925-8388/$ – see front matter © 2010 Elsevier B.V. All rights reserved.
doi:10.1016/j.jallcom.2010.12.132

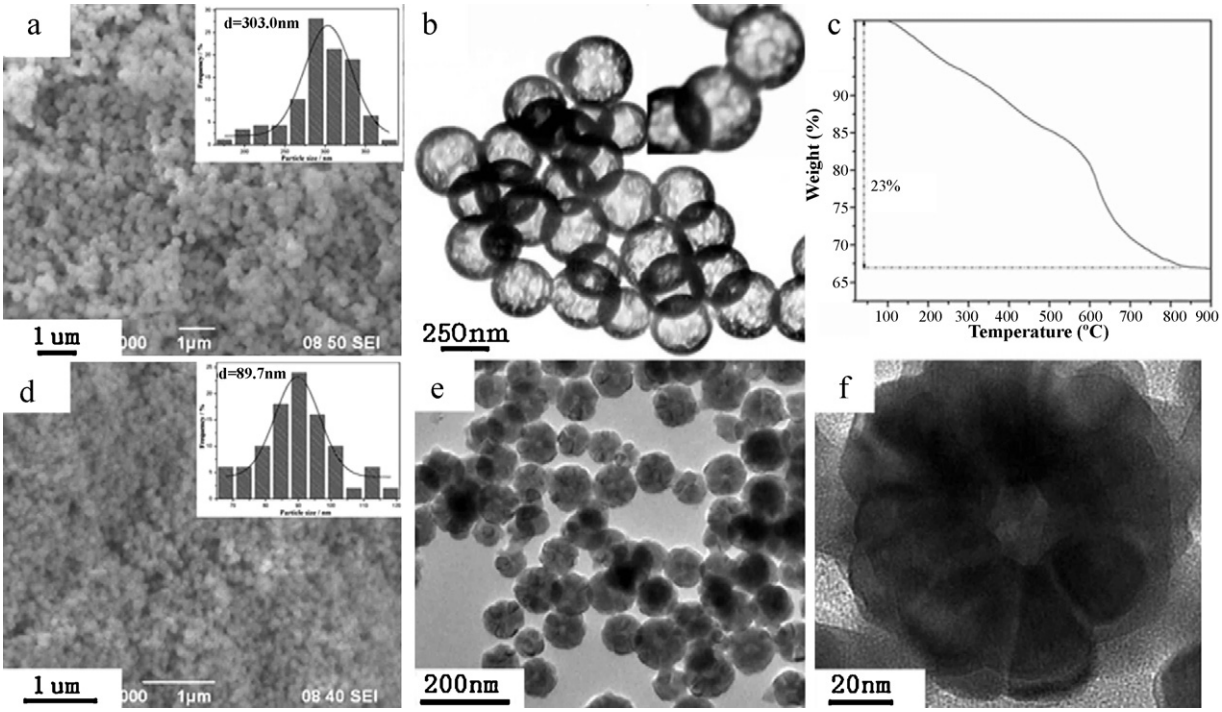

Fig. 1. The precursors synthesized by solvothermal method. (a) SEM image and particle size distribution histogram (inset), (b) TEM image and magnified image (inset) and (c) TG curve. The Y_2O_3:Eu^{3+} hollow spheres obtained through 850 °C calcination. (d) SEM image and particle size distribution histogram (inset), (e) TEM image and (f) magnified TEM image.

the mixture was stirred for 10 min to form homogeneous solution. Subsequently, the obtained solution was transferred into a 100 mL Teflon-lined autoclave, sealed and maintained at 160 °C for 12 h. After the autoclave was cooled to room temperature, the precursors were collected by centrifugation, washed with deionized water and ethanol several times. Finally, the product was dried in vacuum at 60 °C for 4 h.

2.2. Synthesis of Y_2O_3:Eu^{3+} hollow spheres

To fabricate Y_2O_3:Eu^{3+} hollow spheres, the as-prepared precursors were annealed at different temperatures respectively (450 °C, 650 °C, 850 °C, 950 °C) in muffle furnace for 2 h.

2.3. Characterization

X-ray diffraction (XRD) analyses were carried out using a Bruker advance-D_8 XRD with Cu Kα radiation (λ = 0.154178 nm). The accelerating voltage was set at 40 kV with a 100 mA flux. The sizes and morphologies of the resulting products were studied by scanning electron microscopy (SEM) on JEOL JSM-6390LV and by transmission electron microscopy (TEM) on JEOL JSM-100. The room temperature photoluminescence was preformed on JASCO FP-6500 fluorophotometer, the sample was prepared by dispersing 1 mg sample homogeneously into 5 mL ethanol. Fourier transform infrared (FT-IR) spectroscopy spectra were recorded on a Bio-Rad FTS-40 Fourier transform infrared spectrometer in the wave number range of 4000–400 cm^{-1}. Thermogravimetry (TG) of the samples was carried out with a Netzsch STA 409 PC analyzer at a heating rate of 10 °C/min from 20 °C to 900 °C.

3. Results and discussion

The SEM image of hollow precursor is displayed in Fig. 1a and the inset is the corresponding particle size distribution. The precursor consists of uniform spheres with average diameter around 300 nm. Meanwhile, the TEM image of the precursor shows the inner parts of the products are completely hollowed (Fig. 1b). Moreover, as observed from the image inserted in Fig. 1b, the shell is very thin and bubbled with tiny pores. The TG curve of the precursor is shown in Fig. 1c, the precursor starts to decompose at about 100 °C. When the temperature reaches to 850 °C, the overall weight loss is measured to be 23%, which is in accordance with the theoretical weight loss for the conversion from Y(Eu)(OH)CO_3 to Y_2O_3:Eu^{3+}. Fig. 1d shows the SEM image of the final Y_2O_3:Eu^{3+} hollow spheres. After annealed at 850 °C for 2 h, the average size of the final products shrinks to about 90 nm (inset of Fig. 1d). The corresponding TEM image reveals the inner structure of this product. The nano-sized hollow spheres are composed of nanoparticles with diameter of about 20 nm (Fig. 1e). Fig. 1f depicts the detailed structure of an individual hollow sphere and the inner diameter of the hollow sphere is measured to be about 15 nm. This temperature-triggered size shrinkage is previously reported in different works, which is attributed to the crystallization of primary particles and the collapse of the hollow-structured precursor [27–29].

The crystalline structures of the products are studied by XRD. Fig. 2a depicts the XRD patterns of the samples calcined at different temperatures (450–950 °C). It is found that the product still remains amorphous after annealed at 450 °C. However, when the temperature was elevated to 650 °C, 850 °C and 950 °C, all diffraction peaks of these samples could be readily indexed to pure cubic Y_2O_3 (JCPDS Card No. 25-1200). Five main peaks at $2\theta \approx 20.6$, 29.3, 33.9, 48.6, 57.6 are presented in the XRD patterns, which can be assigned to (2 1 1), (2 2 2), (4 0 0), (4 4 0), (0 2 2) reflections of cubic Y_2O_3. No additional peaks were detected indicating the Eu^{3+} cations were effectively built into the host lattice. Fig. 2b shows the XRD patterns of the products obtained at different doping levels with calcining at 850 °C. All of the diffraction peaks could also be well indexed to the cubic Y_2O_3 and there is no impurities belong to Eu_2O_3 existing in the sample, which suggests the Eu element was gracefully doped into the Y_2O_3 lattice. Moreover, the lattice parameters of the products were calculated according to the equation of $1/d^2 = (h^2 + k^2 + l^2)/a^2$ (based on the crystal plane of (2 2 2)). The a-values of these products are well compatible with the standard value of a = 1.0604 nm (JCPDS No. 25-1200), which confirms that the Eu^{3+} ions are readily doped into the host lattice.

In order to reveal the formation process, time-dependent experiments were carried out by collecting intermediate products at different intervals: 15 min, 2 h and 6 h. Afterwards, these products were analyzed by TEM (Fig. 3). When the reaction was carried out for 15 min, only aggregated particles with diameter about several

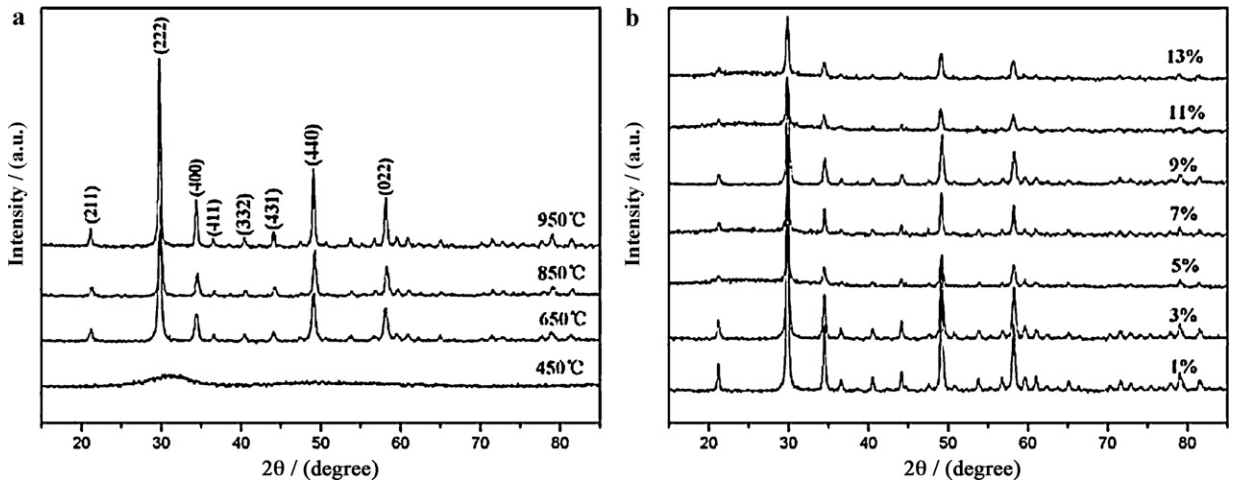

Fig. 2. XRD patterns for (a) Y_2O_3:Eu^{3+} (9 mol%) obtained at different calcination temperatures; (b) Y_2O_3:Eu^{3+} with different doping levels through calcining at 850 °C.

nanometers could be detected (Fig. 3a). If the reaction was prolonged to 2 h (Fig. 3b), hollow spheres with outer diameter around 200 nm were formed and the shell thickness was measured to be about 40–50 nm. As shown in Fig. 3c, hollow spheres still existed when the reaction was further elevated to 6 h. However, compared with the hollow structure generated after 2 h, the outer diameter experienced a slight growth but the shell thickness was reduced. Finally, when the reaction time reached to 12 h, the shell thickness became much thinner, meanwhile, the outer diameter still remained unchanged (Fig. 1b).

On the basis of the morphology evolution collected in the time-dependent experiments, a possible growth mechanism was proposed. In our work, no additional reagent is used as template. Most probably, the bubbles of CO_2 gas generated by the decomposition of urea played a crucial role in forming the hollowed precursor. Firstly, urea decomposes in the reaction system and produces NH_4^+, OH^- and CO_2. The released OH^- enhances the pH value of the reaction system and leads to the nucleation of precursor. At the same time, the CO_2 bubbles generated from the hydrolyzed urea may serve as template to direct the formation of the hollow structure (Fig. 3d) [30]. For comparison, a control experiment was also conducted using $NH_3{\cdot}H_2O$ as precipitator, which provided a similar reaction surrounding except the CO_2 bubbles. Finally, only solid aggregate particles with diameter of about 200 nm were observed in the product, which further confirms the role of CO_2 in directing the hollow structure. Afterward, the primary particle assembled along the gas and liquid interface to form hollow aggregated spheres with greater shell thickness. At this stage, the mixed solvent of water and ethanol also played a significant part in forming the hollow precursor by offering the reaction system with a suitable polarity. Pure water or absolute ethanol was respectively applied as the reaction media for comparison, but no hollow spherical product was generated. According to Zeng's work, the particles located at the inner surface of the hollow sphere are of higher free energy than that of the outer surface, which leads to the gradual dissolving of the inner particles and re-growth at

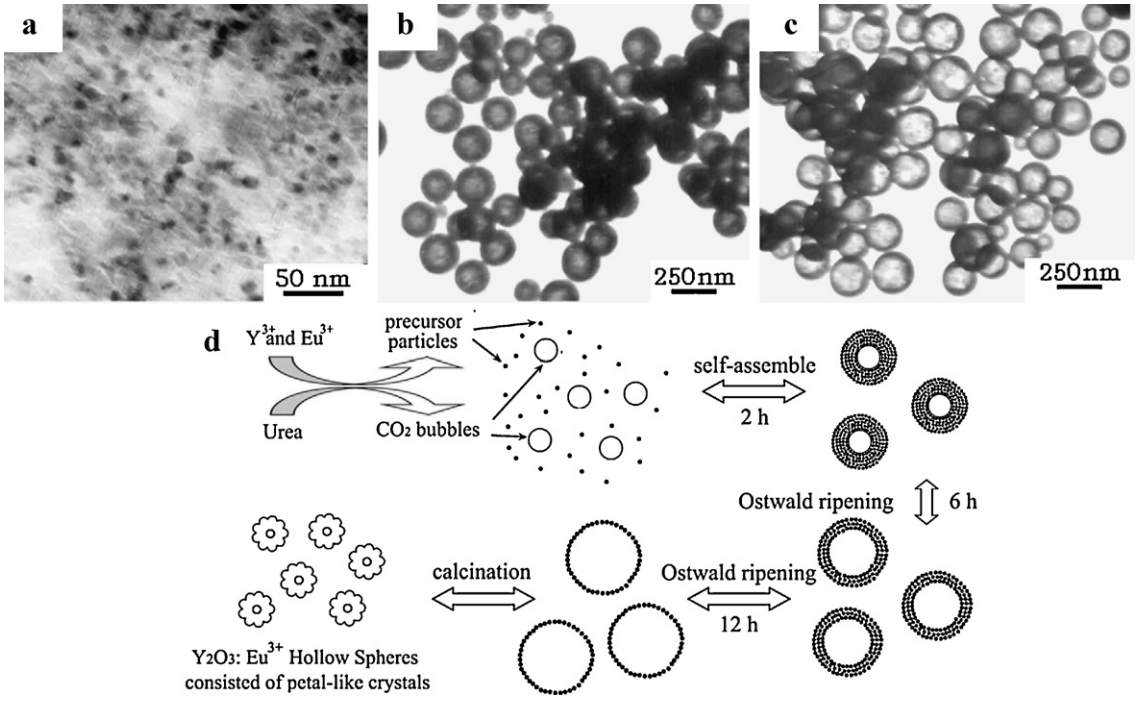

Fig. 3. TEM images of hollow spherical precursor with different time intervals (a) 15 min, (b) 2 h, and (c) 6 h at 160 °C. (d) Schematic illustration of growth process.

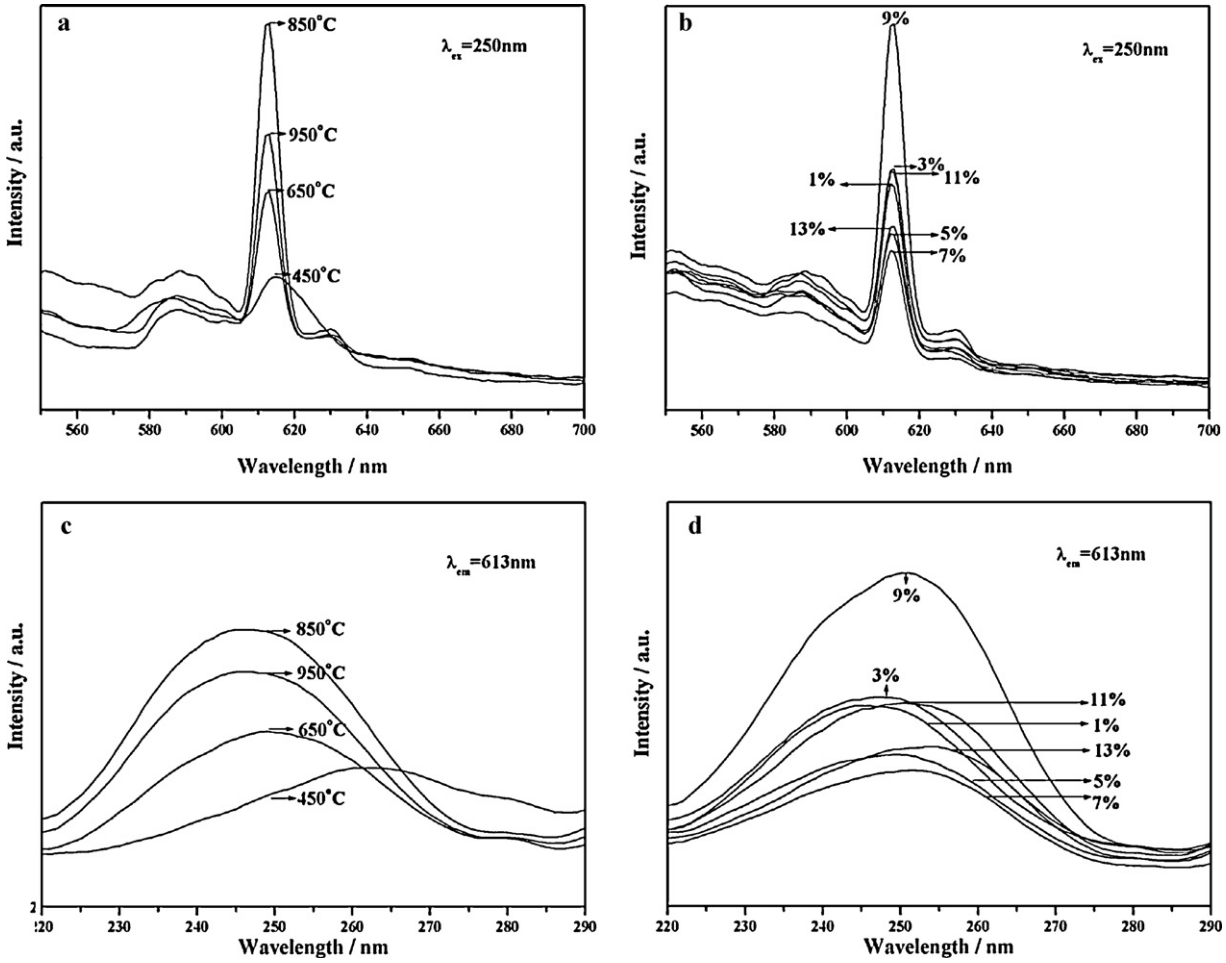

Fig. 4. Emission spectra of the products obtained at different conditions: (a) products obtained at different calcining temperatures with same Eu^{3+} doping level (9 mol%); (b) products obtained at different doping levels with same calcination temperature (850 °C). Excitation spectra of the Y_2O_3:Eu^{3+} obtained at (c) different calcining temperatures; (d) different doping levels.

the outer surface [31]. Therefore, during the reaction, the diameter of the hollow sphere became greater and the shell thickness was reduced, which could be also defined as an Ostwald ripening controlled process. Finally, the precursor was annealed to generate the final Y_2O_3:Eu^{3+} hollow spheres. The size shrinking from precursor (about 300 nm) to the final product (about 90 nm) probably derives from the crystallization of the primary particles and the collapsing of hollow precursor. This formation process generally involves the assembling of the primary particles and the later Ostwald ripening growth, which is schematically illustrated in Fig. 3d.

Fig. 4 shows the PL emission spectra of Y_2O_3:Eu^{3+} products obtained at different conditions excited by a 250 nm laser. Fig. 4a depicts the spectra of the samples prepared at different calcination temperatures with same Eu^{3+} doping level (9 mol%). The emission spectra consist of lines in the red spectral area, which correspond to the transitions from the excited $^5D_0$ level to ^7F_J (J=0, 1, 2, 3, 4, not in all cases) level of Eu^{3+} ion. For all samples, the dominating emission peak is located at around 613 nm which is caused by the hypersensitive forced electric dipole transition ($^5D_0 \rightarrow {}^7F_2$). Furthermore, the PL emission intensity enhanced greatly with increasing the calcining temperature from 450 °C to 850 °C, because a higher calcining temperature results in better crystallinity which permits a better activation for the doped Eu^{3+} ions. However, the emission intensity experienced a slightly decrease when the calcining temperature was elevated to 950 °C. Under an extreme high temperature, more defects may occur in the crystal structure and the temperature could also destroy the hollow structure of the product, which finally leads to the decrease of the PL intensity [32–36]. Therefore, 850 °C is the optimum calcination temperature to present the best luminescence performance. Fig. 4b displays the emission spectra of the products with different doping levels. All peaks are centered at 613 nm and the peak positions remain unchanged as the variation of Eu^{3+}, indicating the nature of the europium activation was not affected by the doping concentration. Moreover, the peak intensity fluctuated when the Eu^{3+} doping level was tuned from 1 mol% to 13 mol%. The results suggest the optimum doping concentration is 9 mol% and this doping level is higher than those obtained from the conventional methods, which may result in a better luminescence performance [37,38]. When the doping level was higher than 9 mol%, the PL emission intensity gradually decreases as the Eu^{3+} ion doping level is elevated. This decrease should be resulting from the concentration quenching which was caused by the cross-relaxation between neighboring Eu^{3+} ions [39].

The excitation spectrum was obtained by monitoring the emission of $^5D_0 \rightarrow {}^7F_2$ transition of the Eu^{3+} at 613 nm (Fig. 4c and d). The excitation spectrum consists of a broad band with a maximum at about 250 nm, which corresponds to the charge transfer transition from the 2p orbital of O^{2-} to the 4f orbital of Eu^{3+} [40]. Moreover, from the excitation spectrum of the as-prepared particles at different calcination temperatures (Fig. 4c) and different doping levels (Fig. 4d), the products prepared at 850 °C with 9 mol% doping level shows the highest excitation peak, indicating the electron transfer from the 2p orbital of O^{2-} to the 4f orbital of Eu^{3+} was

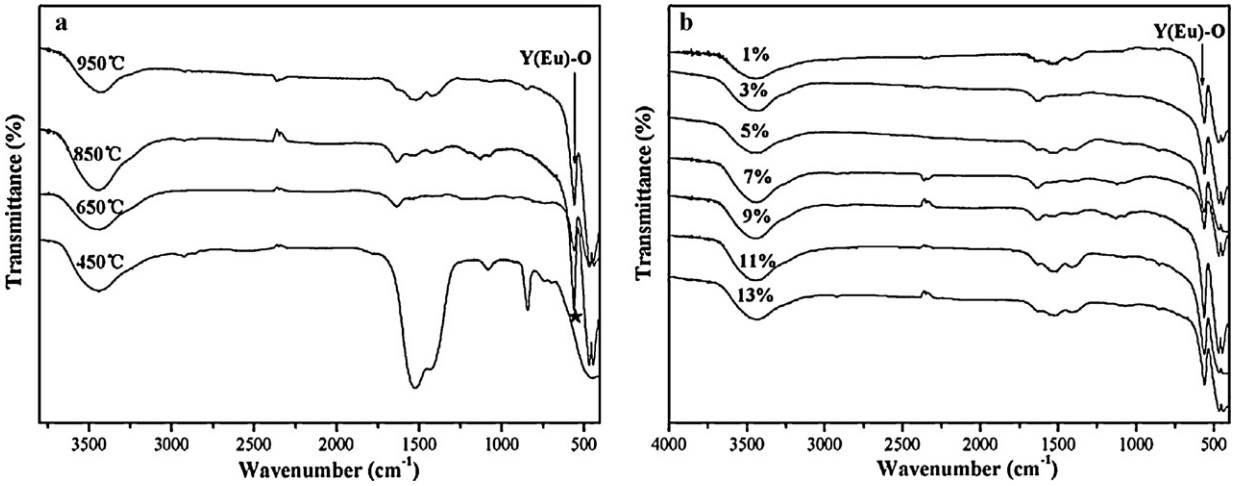

Fig. 5. FT-IR spectra (a) Y_2O_3:Eu^{3+} (9 mol%) prepared at different calcining temperatures (b) Y_2O_3:Eu^{3+} with different doping level prepared at 850 °C.

promoted under this conditions, which results in its enhanced PL performance.

In order to investigate the relation between the surface groups and optical property of the as-prepared Y_2O_3:Eu^{3+}, FT-IR spectra of the products were analyzed. Fig. 5a shows the spectra of the products calcinated at different temperatures. The FT-IR spectra generally consisted of two parts: the first part is attributed to the absorption of CO_3^{2-}, including the peak at 844 cm^{-1} arising from the deformation vibration of C–O and the peaks at 1434 and 1528 cm^{-1} due to C–O asymmetric stretching. The second part is the broad peak at 3343 cm^{-1}, which are assigned to the O–H vibration. The sample obtained at 450 °C has absorption bands at 3443, 1434, 1528, 1081, 844, 742, and 696 cm^{-1}, which can be attributed to (υ = stretch; υ_s = symmetric stretch; υ_{as} = asymmetric stretch; δ = deformation) OH (υ), CO (υ_{as}), CO (υ_{as}), CO (υ_s), CO (δ), OH (δ), and CO (δ), respectively. According to previous reports, this result indicates that the formula of the precursor could be assigned to Y(Eu)(OH)CO_3 [5,41]. However, when the precursor was annealed under temperature above 450 °C, the absorption peaks from the organic components decrease, peaks at 844 cm^{-1}, 1434 cm^{-1} and 1528 cm^{-1} become weaker. On the other hand, three new bands peaking at 444, 467 and 561 cm^{-1} appear, which are corresponding to the absorption of Y(Eu)–O peak revealing the formation of Y_2O_3:Eu^{3+}. According to Wang's work [40], these three peaks can work as an indicator for the Eu^{3+} doping effect, a higher intensity suggests a stronger doping effect which could results in enhanced PL performance. When annealed at 850 °C, the sample has a stronger absorption peak at 444, 467 and 561 cm^{-1} in the FT-IR spectra than the samples prepared under other temperatures (Fig. 5a). Similarly, when the doping level was 9 mol%, the product has stronger absorption peaks than other samples, which means this concentration could result in a better doping effect (Fig. 5b). Therefore, when the products were prepared at 850 °C and with 9 mol% doping level, the Eu^{3+} ions have the best doping effect and the strongest interaction between the atom of Eu and the host matrix atom (Y and O), which is believed to make positive contribution to its enhanced luminescence performance.

4. Conclusions

In summary, a facile template-free method was developed to fabricate uniform Y(Eu)(OH)CO_3 hollow spheres with high yield. Moreover, urea and the mixed solvent were found to be the two crucial factors in producing the hollow precursors. Afterwards, nano-sized Y_2O_3:Eu^{3+} hollow spheres were prepared by annealing the precursor in air. Additionally, we intensively studied the optical property of the novel Y_2O_3:Eu^{3+} structure. The as-prepared Y_2O_3:Eu^{3+} products exhibit a strong red emission at 613 nm corresponding to the $^5D_0 \rightarrow {}^7F_2$ transition of the Eu^{3+} ions and the optimal preparation condition is calcinated at 850 °C with Eu^{3+} doping level of 9 mol%. The improved luminescence performance is found to associate with the interaction between the Eu^{3+} ions and the Y_2O_3 host matrix which could be confirmed by the FT-IR investigation. Finally considering the excellent red emission property, this unique material could be potentially utilized in the fields such as light phosphor powders, flat panel displays, and biological labeling.

Acknowledgments

This work was supported by the National Natural Science Foundation of China (20571025) and Henan Innovation Project for University Prominent Research Talents (2005KYCX005).

References

[1] J. Su, Q.L. Zhang, S.F. Shao, W.P. Liu, J. Alloys Compd. 470 (2009) 306–310.
[2] G. Jia, H. You, Y. Song, Y. Huang, M. Yang, H. Zhang, Inorg. Chem. 49 (2010) 7721–7725.
[3] L. Muresan, E.J. Popovici, R. Grecu, L.B. Tudoran, J. Alloys Compd. 471 (2009) 421–427.
[4] Y.X. Fu, Y.H. Sun, J. Alloys Compd. 471 (2009) 190–196.
[5] G. Jia, M. Yang, Y. Song, H. You, H. Zhang, Cryst. Growth Des. 9 (2009) 301–307.
[6] X. Hou, S. Zhou, Y. Li, W. Li, J. Alloys Compd. 494 (2010) 382–385.
[7] V.B. Taxak, S.P. Khatkar, S.D. Hanb, R. Kumara, M. Kumara, J. Alloys Compd. 469 (2009) 224–228.
[8] A.P. Jadhav, A. Pawar, C.W. Kim, H.G. Cha, U. Pal, Y.S. Kang, J. Phys. Chem. C 113 (2009) 16652–16657.
[9] Y.P. Fu, S.B. Wen, C.S. Hsu, J. Alloys Compd. 458 (2008) 312–318.
[10] K.M. Nissamudeen, K.G. Gopchandran, J. Alloys Compd. 490 (2010) 399–406.
[11] X. Li, Q. Li, Z. Xia, L. Wang, W. Yan, J. Wang, R.I. Boughton, Cryst. Growth Des. 6 (2006) 2193–2196.
[12] S. Zhong, J. Chen, S. Wang, Q. Liu, Y. Wang, S. Wang, J. Alloys Compd. 493 (2010) 322–325.
[13] P. Leidinger, R. Popescu, D. Gerthsen, C. Feldmann, Small 6 (2010) 1886–1891.
[14] X. Wang, F. Wan, J. Liu, Y. Gao, K. Jiang, J. Alloys Compd. 474 (2009) 233–236.
[15] Y. Wang, G. Wang, H. Wang, C. Liang, W. Cai, L. Zhang, Chem. Eur. J. 16 (2010) 3497–3503.
[16] S. Hosokawa, S. Iwamoto, M. Inoue, J. Alloys Compd. 457 (2008) 510–516.
[17] S. Gurmen, B. Ebin, J. Alloys Compd. 492 (2010) 585–589.
[18] H.G. Yang, H.C. Zeng, Angew. Chem. Int. Ed. 43 (2004) 5930–5933.
[19] L. Yang, W. Guan, B. Bai, Q. Xu, Y. Xiang, J. Alloys Compd. 504 (2010) L10–L13.
[20] L. Zhang, H. Yang, X. Xie, F. Zhang, L. Li, J. Alloys Compd. 473 (2009) 65–70.
[21] C. Zhang, C. Li, C. Peng, R. Chai, S. Huang, D. Yang, Z. Cheng, J. Lin, Chem. Eur. J. 16 (2010) 5672–5680.
[22] C.H. Chen, S.F. Abbas, A. Morey, S. Sithambaram, L.P. Xu, H.F. Garces, W.A. Hines, S.L. Suib, Adv. Mater. 20 (2008) 1205–1209.
[23] L. Chen, H. Dai, Y. Shen, J. Bai, J. Alloys Compd. 491 (2010) L33–L38.

[24] G. Li, F. Liu, Z. Zhang, J. Alloys Compd. 493 (2010) L1–L7.
[25] H.S. Roh, Y.C. Kang, H.D. Park, S.B. Par, Appl. Phys. A 76 (2003) 241–245.
[26] G. Liu, G. Hong, J. Solid State Chem. 178 (2005) 1647–1651.
[27] X.C. Wu, Y.R. Tao, F. Gao, L. Dong, Z. Hu, J. Cryst. Growth 277 (2005) 643–649.
[28] J. Yang, C.K. Lin, Z.L. Wang, J. Lin, Inorg. Chem. 45 (2006) 8973–8979.
[29] J. Yang, Z. Quan, D. Kong, X. Liu, J. Lin, Cryst. Growth Des. 7 (2007) 730–735.
[30] L.P. Zhu, G.H. Liao, Y. Yang, H.M. Xiao, J.F. Wang, S.Y. Fu, Nanoscale Res. Lett. 4 (2009) 550–557.
[31] H.G. Yang, H.C. Zeng, J. Phys. Chem. B 108 (2004) 3492–3495.
[32] P. Zhou, X. Yu, L. Yang, S. Yang, W. Gao, J. Lumin. 124 (2007) 241–244.
[33] Y. Liu, C.N. Xu, H. Chen, H. Tateyama, J. Lumin. 97 (2002) 135–140.
[34] Q.Y. Zhang, K. Pita, W. Ye, W.X. Que, C.H. Kam, Chem. Phys. Lett. 356 (2002) 161–167.
[35] M.G. Kwak, J.H. Parkb, S.H. Shon, Solid State Commun. 130 (2004) 199–201.
[36] P.K. Sharma, M.H. Jilavi, R. Nass, H. Schmidt, J. Lumin. 82 (1999) 187–193.
[37] S.H. Shin, J.H. Kang, D.Y. Jeon, S.H. Choi, S.H. Lee, Y.C. You, D.S. Zang, Solid State Commun. 135 (2005) 30–33.
[38] Q. Pang, J. Shi, Y. Liu, D. Xing, M. Gong, N. Xu, Mater. Sci. Eng. B 103 (2003) 57–61.
[39] W.C. Chien, J. Cryst. Growth 290 (2006) 554–559.
[40] W.N. Wang, W. Widiyastuti, T. Ogi, I.W. Lenggoro, K. Okuyama, Chem. Mater. 19 (2007) 1723–1730.
[41] M.I. Martinez-Rubio, T.G. Ireland, G.R. Fern, J. Silver, M.J. Snowden, Langmuir 17 (2001) 7145–7149.